Strawberry notch homologue 2 regulates osteoclast fusion by enhancing the expression of DC-STAMP

Kenta Maruyama,[1] Satoshi Uematsu,[1,2] Takeshi Kondo,[1] Osamu Takeuchi,[1,3] Mikaël M. Martino,[1] Takumi Kawasaki,[1] and Shizuo Akira[1]

[1]Laboratory of Host Defense, WPI Immunology Frontier Research Center (IFReC), Research Institute for Microbial Diseases, Osaka University, Suita, Osaka 565-0871, Japan
[2]Division of Innate Immune Regulation, International Research and Development Center for Mucosal Vaccine, Institute for Medical Science, University of Tokyo, Tokyo 108-8639, Japan
[3]Laboratory of Infection and Prevention, Institute for Virus Research, Kyoto University, Kyoto 606-8507, Japan

Osteoclasts are multinucleated cells formed by fusion of mononuclear precursors in response to receptor activator of nuclear factor κB (NF-κB) ligand (RANKL). We found that RANKL induced expression of the DExD/H helicase family corepressor strawberry notch homologue 2 (Sbno2). Previous in vitro studies showed that Sbno2 is induced by IL-10 and is involved in NF-κB repression. However, the role of Sbno2 in vivo and its pleiotropic functions are unknown. *Sbno2* gene targeting resulted in normal NF-κB activation by TLR ligands. However, Sbno2-deficient mice exhibited increased bone mass due to impaired osteoclast fusion. Expression of dendritic cell–specific transmembrane protein (DC-STAMP), a critical player in osteoclast fusion, was significantly attenuated, and cell fusion of Sbno2-deficient osteoclasts was rescued by DC-STAMP. Sbno2 directly bound to T cell acute lymphocytic leukemia 1 (Tal1) and attenuated its inhibition of DC-STAMP expression, leading to activation of the DC-STAMP promoter by microphthalmia-associated transcription factor (MITF). Thus, Sbno2 plays a pivotal role in bone homeostasis in vivo by fine-tuning osteoclast fusion.

CORRESPONDENCE
Shizuo Akira:
sakira@biken.osaka-u.ac.jp.

Abbreviations used: ALP, alkaline phosphatase; CTSK, cathepsin K; DC-STAMP, DC-specific transmembrane protein; MDM, M-CSF–derived macrophage; MITF, microphthalmia-associated transcription factor; MNC, multinuclear cell; MSC, mesenchymal stem cell; μ-CT, microcomputed tomographic; RANKL, receptor activator of NF-κB ligand; Sbno2, strawberry notch homologue 2; Tal1, T cell acute lymphocytic leukemia 1; TRACP 5b, TRAP 5b; TRAP, tartrate-resistant acid phosphatase.

Osteoporosis is a serious disease among postmenopausal women and elderly people in developed countries, which can lead to bone fractures. In the elderly population, spine and hip fractures are chronic diseases characterized by an abnormal balance in the activities of osteoclasts and osteoblasts (Khosla, 2009).

Osteoclasts are multinucleated cells that are derived from the myeloid lineage (Karsenty and Wagner, 2002). Bone-forming osteoblasts express macrophage-CSF (M-CSF) and receptor activator of NF-κB ligand (RANKL). When these cytokines stimulate their receptors, c-fms and RANK, respectively, transcription factors such as c-Fos (Grigoriadis et al., 1994), Jdp2 (Kawaida et al., 2003; Maruyama et al., 2012a), microphthalmia-associated transcription factor (MITF; Motyckova et al., 2001), NFATc1 (Takayanagi et al., 2002), and NF-κB (Franzoso et al., 1997) in osteoclast precursors are activated and osteoclast differentiation is induced by induction of osteoclastic genes such as tartrate-resistant acid phosphatase (TRAP), cathepsin K (CTSK), and DC-specific transmembrane protein (DC-STAMP). Among osteoclastic genes, DC-STAMP is a crucial factor for osteoclast fusion because cells from DC-STAMP–deficient mice cannot develop multinucleated osteoclasts, and consequently, resorption pit formation is inhibited (Yagi et al., 2005). It was recently reported that an anti–DC-STAMP monoclonal antibody strongly blocked osteoclast formation in vitro (Chiu et al., 2012). Expression of DC-STAMP is positively regulated by MITF (Courtial et al., 2012). Furthermore, T cell acute lymphocytic leukemia 1 (Tal1) represses DC-STAMP expression by counteracting the activation function of MITF (Courtial et al., 2012). Collectively, these findings suggest that osteoclast fusion is orchestrated by complex interplay between several transcription factors.

The Rockefeller University Press $30.00
J. Exp. Med. 2013 Vol. 210 No. 10 1947-1960
www.jem.org/cgi/doi/10.1084/jem.20130512

The Journal of Experimental Medicine

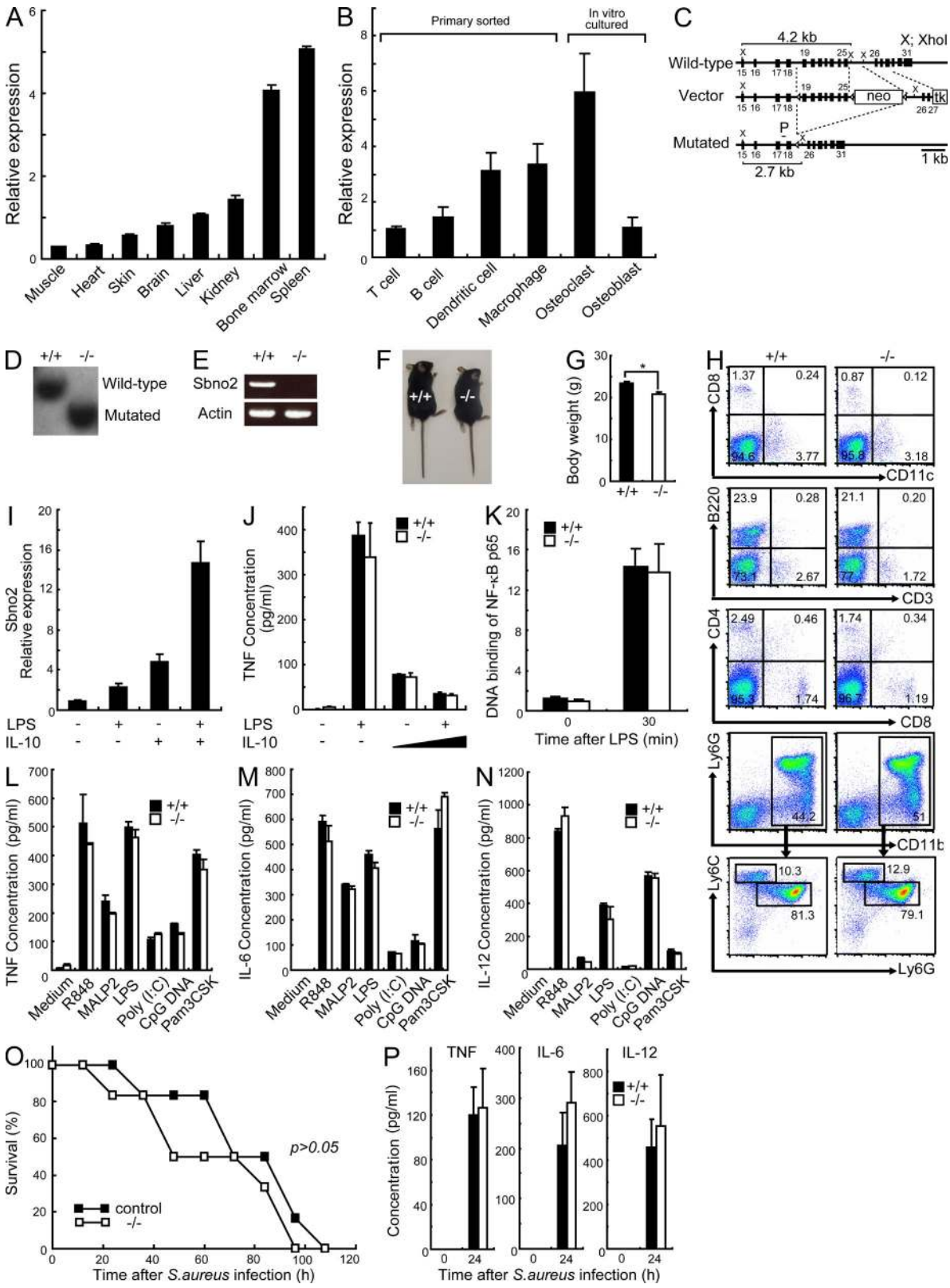

Figure 1. Sbno2 is dispensable for TLR signaling. (A and B) The indicated organs (A) or hematopoietic cells (B) were harvested from wild-type mice and Sbno2 expression was analyzed by qPCR. (C) Structure of the *Sbno2* gene, targeting vector, and predicted mutated allele. Open triangles indicate loxP sites. Closed boxes and numbers represent exons and exon numbers, respectively. P indicates the probe for Southern blotting. (D) Southern blotting analysis of the offspring from heterozygote intercrosses. DNA was digested with XhoI and hybridized with the probe indicated in C. (E) RNA was extracted from

Other than RANKL, various cytokines and pathogen-associated molecules are known to activate NF-κB. NF-κB controls the expression of proinflammatory cytokines in response to pathogenic infection downstream of TLR (Akira et al., 2006). In contrast, IL-10 receptor signaling activates STAT3 and enhances the antiinflammatory response (Takeda et al., 1999). Recently, it was reported that IL-10 induces expression of the DExD/H helicase family corepressor strawberry notch homologue 2 (Sbno2) in a STAT3-dependent manner. Importantly, according to a luciferase reporter assay, Sbno2 represses NF-κB but not IRF7 (El Kasmi et al., 2007). Thus, these findings indicate that Sbno2 is a negative regulator of the proinflammatory cascade.

Despite its importance in NF-κB activation, the in vivo role of Sbno2 and its pleiotropic functions are largely uncharacterized. Here, we report the in vivo function of Sbno2 in fine-tuning osteoclast fusion by regulating DC-STAMP expression.

RESULTS

Sbno2 is dispensable for NF-κB activation

Sbno2 was found to be expressed in the spleen and bone marrow, and to a lesser extent in the kidney, liver, brain, skin, heart, and muscle (Fig. 1 A). Such findings indicate that Sbno2 is predominantly expressed in the hematopoietic system. Thus, we next examined the expression of Sbno2 in various hematopoietic cell types. Sbno2 expression levels in myeloid cells were significantly higher compared with those in T cells, B cells, and osteoblasts (Fig. 1 B). Among the myeloid cells, Sbno2 expression was highest in osteoclasts (Fig. 1 B). Therefore, we focused on the role of Sbno2 in myeloid lineages. To evaluate Sbno2 function, *Sbno2*$^{-/-}$ mice were generated (Fig. 1, C–E) and the Sbno2 genotypes of offspring derived from heterozygous intercrosses are analyzed. We genotyped these offspring and observed a distribution of 28.2% +/+, 52.4% +/−, and 19.4% −/−. Because no resorption of fetuses was observed (unpublished data), this distribution is enigmatic in view of the Mendelian ratio. To elucidate the cause of this abnormality, we analyzed the sex of offspring. The same numbers of male and female mice were observed among offspring derived from heterozygous intercrosses. Furthermore, female offspring were born in the expected Mendelian ratio. In contrast, the genotype distribution of male offspring was 30.8% +/+, 53.8% +/−, and 15.4% −/− (unpublished data). This ratio implies the existence of distorted male transmission.

Apparent macro-morphological abnormalities were not observed (Fig. 1 F), although *Sbno2*$^{-/-}$ mice exhibited slightly decreased body weight at 10 wk of age (Fig. 1 G). We also evaluated the bone marrow population of lymphoid and myeloid cells in *Sbno2*$^{-/-}$ mice (Fig. 1 H), revealing that lineage development appeared to be normal in these mice. As previously reported, Sbno2 expression in M-CSF–derived macrophages (MDMs) was induced by LPS or IL-10, and was synergistically induced by both stimuli (Fig. 1 I). Thus, we next examined the ability of IL-10 to inhibit LPS-induced TNF production in wild-type and *Sbno2*$^{-/-}$ MDMs. However, in contrast to our expectations, the suppressive effect of IL-10 on TNF production appeared to be comparable between wild-type and *Sbno2*$^{-/-}$ MDMs (Fig. 1 J). Furthermore, Sbno2 deficiency did not alter NF-κB activation (Fig. 1 K) or proinflammatory cytokine production in response to various TLR ligands in MDMs (Fig. 1, L–N) and GM-CSF–induced conventional DCs (not depicted). We also intravenously infected *Sbno2*$^{-/-}$ and wild-type mice with *Staphylococcus aureus* to investigate whether Sbno2 had an effect on sepsis. As expected, Sbno2 deficiency had no effect on survival or proinflammatory cytokine production in response to in vivo *S. aureus* acute infection (Fig. 1, O and P). Thus, these findings clearly indicate that Sbno2 is dispensable for NF-κB activation and cytokine production both in vivo and in vitro.

Sbno2$^{-/-}$ mice are osteopetrotic

At 4 wk of age, we observed no bone histomorphometric abnormality in *Sbno2*$^{-/-}$ mice (Fig. 2, A–C). While flushing bone marrow cells from 10-wk-old mouse femurs to generate MDMs, we noticed that the femurs from *Sbno2*$^{-/-}$ mice appeared to be stronger than those from wild-type mice. Such findings prompted us to precisely explore the role of Sbno2 in skeletal systems. Microcomputed tomographic (μ-CT) analysis of femurs showed that *Sbno2*$^{-/-}$ mice had osteopetrosis accompanied by a marked increase in trabecular bone volume and number compared with wild-type mice (Fig. 2, D and E). Histological sections of proximal tibias from *Sbno2*$^{-/-}$ mice also exhibited increased trabecular bone volume and number (Fig. 2, F and G). Histomorphometric analysis revealed a significant reduction in the osteoclast surface/bone surface and eroded surface/bone surface ratio, but the osteoclast number/bone surface ratio was normal in *Sbno2*$^{-/-}$ mice (Fig. 2, H and I).

wild-type and *Sbno2*$^{-/-}$ MDMs, and Sbno2 mRNA levels were measured by PCR. (F) Representative photographs of wild-type and *Sbno2*$^{-/-}$ mice. (G) Body weights of 11-wk-old wild-type and *Sbno2*$^{-/-}$ mice (*, $P < 0.05$; $n = 4$). (H) Bone marrow cells were prepared from wild-type and *Sbno2*$^{-/-}$ mice, stained with the indicated antibodies, and analyzed by FACS. (I) MDMs from wild-type and *Sbno2*$^{-/-}$ mice were cultured with LPS alone, IL-10 alone, or LPS plus IL-10 for 2 h. Sbno2 expression was analyzed by qPCR. (J) MDMs from wild-type and *Sbno2*$^{-/-}$ mice were precultured with increasing concentrations of IL-10 for 18 h, and then incubated with LPS for 12 h. TNF concentrations were measured by ELISA. (K) The DNA-binding activity of NF-κB in response to LPS was measured using a TransAM Transcription Factor Assay kit. (L–N) Wild-type and *Sbno2*$^{-/-}$ MDMs were stimulated with various TLR ligands (20 ng/ml Pam3CSK, 300 μg/ml Poly(I:C), 100 ng/ml LPS, 50 nM R848, or 100 nM CpG DNA) for 12 h. Supernatant TNF (L), IL-6 (M), and IL-12 (N) levels were measured by ELISA. (O) *S. aureus* was intravenously injected into wild-type and *Sbno2*$^{-/-}$ mice. Survival was monitored for 120 h after infection ($n = 6$). (P) Serum cytokine levels were determined at 24 h after *S. aureus* infection. Results are representative of three (A, B, and I–N) or two (O and P) independent experiments. Error bars, SE. $n = 3$, unless indicated.

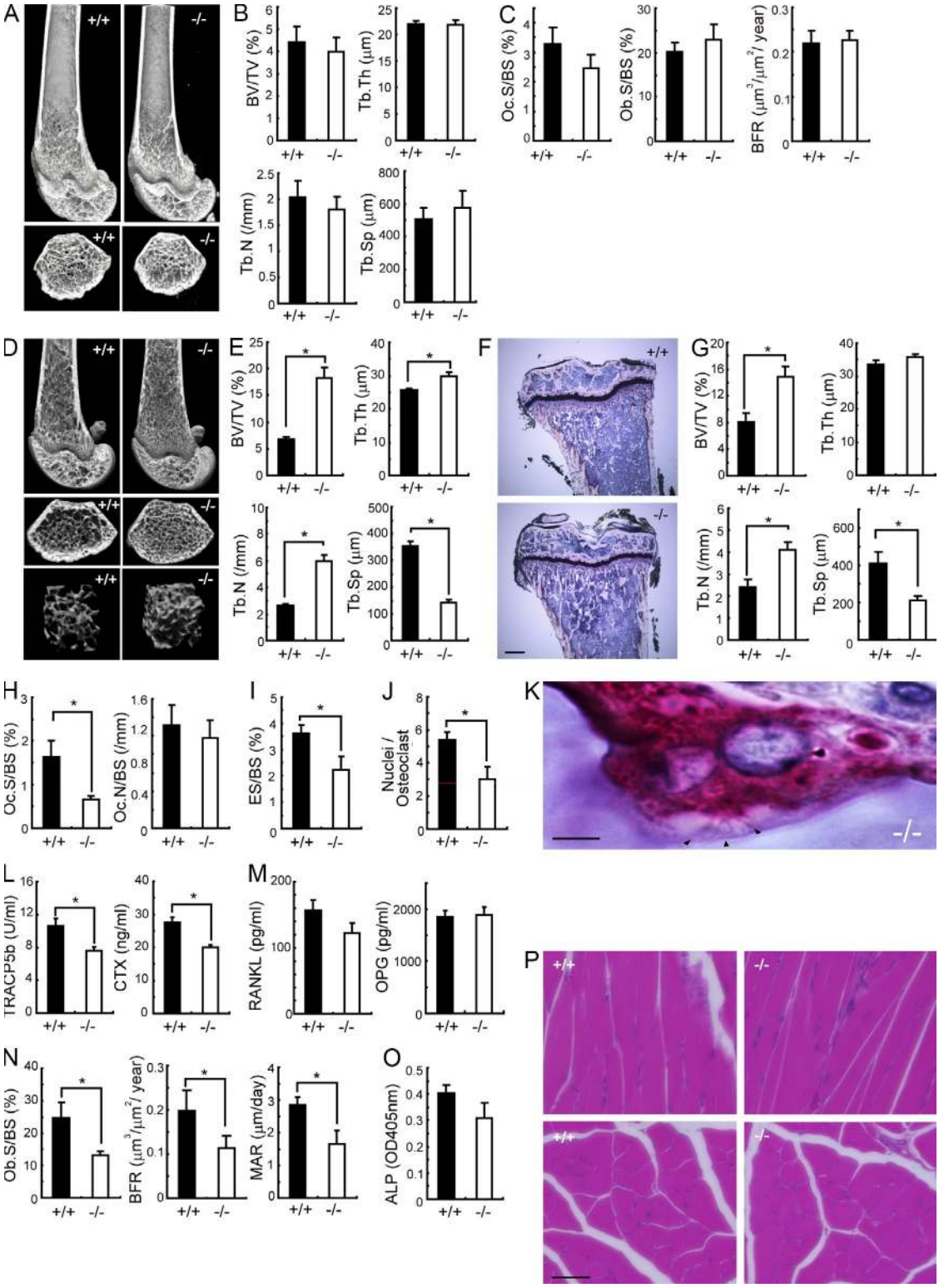

Figure 2. Osteopetrotic phenotype of 10-wk-old *Sbno2*$^{-/-}$ mice. (A) Representative μ-CT images of distal femurs from 4-wk-old *Sbno2*$^{-/-}$ mice (top: longitudinal view; bottom: axial view of the metaphyseal region). (B) Bone morphometric analysis of femurs from A using μ-CT. (C) Osteoclast and bone formation parameters in the metaphyseal portion in the metaphyseal portion of tibias. Oc.S/BS, osteoclast surface per bone surface; BFR, bone formation rate. (D) Representative μ-CT images of distal femurs from 10-wk-old wild-type and *Sbno2*$^{-/-}$ mice (top: longitudinal view; middle: axial view of the metaphyseal region; bottom: three-dimensional view of the metaphyseal region). (E) Bone morphometric analysis of distal femurs using μ-CT. (F) Representative proximal portion of tibias. Bar, 0.5 mm. (G) Bone morphometric analysis of proximal tibias. (H) Osteoclast parameters in the metaphyseal portion of tibias from wild-type

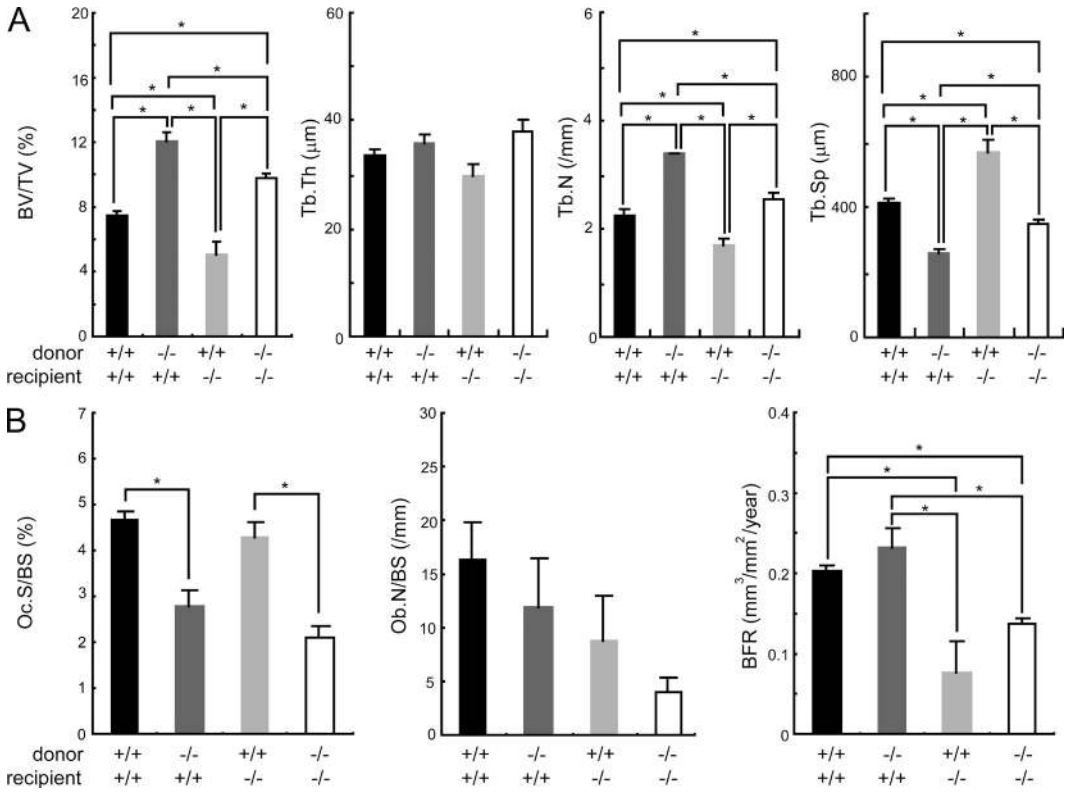

Figure 3. Increased bone mass in *Sbno2*$^{-/-}$ mouse is solely due to osteoclasts. (A) 4-wk-old wild-type or *Sbno2*$^{-/-}$ mice were radiated and reconstituted with bone marrow from wild-type or *Sbno2*$^{-/-}$ mice. After 7 wk, bone morphometric analysis of proximal tibias was performed. (B) Osteoclast and osteoblast parameters from proximal tibias in A. BV/TV, bone volume per tissue volume; Tb.Th, trabecular bone thickness; Tb.N, trabecular bone number; Tb.Sp, trabecular bone spacing. Oc.S/BS, osteoclast surface per bone surface; Ob.N/BS, osteoblast number per bone surface; Ob.S/BS, osteoblast surface per bone surface; BFR, bone formation rate. Error bars, SE. *, $P < 0.05$, $n = 3$–4/group. Results are representative of two independent experiments.

We also confirmed that the nuclei/osteoclast ratio was decreased in *Sbno2*$^{-/-}$ mice (Fig. 2 J). In contrast, ruffled border formation was normally observed in *Sbno2*$^{-/-}$ osteoclasts (Fig. 2 K). These findings indicate that osteoclast fusion, but not differentiation, might be diminished in *Sbno2*$^{-/-}$ mice. Consistently, serum bone resorption marker levels of TRAP 5b (TRACP5b) and serum type 1 collagen cross-linked C-terminal telopeptide (CTX) were lower in *Sbno2*$^{-/-}$ mice than those in wild-type mice (Fig. 2 L). Furthermore, serum levels of RANKL and alkaline phosphatase (ALP) were slightly, but not significantly, impaired (Fig. 2, M and O). Notably, *Sbno2*$^{-/-}$ mice exhibited a slight and significant decrease in osteoblast surface/bone surface ratio, bone formation rate, and mineral apposition rate (Fig. 2 N). It has been well known that myotubes fuse to form myofibers, but Sbno2-deficient mice exhibited no morphological abnormality in femoral muscles (Fig. 2 P), indicating that cellular fusion of myotubes was normal. Next, to evaluate the importance of the osteoclastic Sbno2 deficiency to increased bone mass, we irradiated wild-type mice and reconstituted them with bone marrow from wild-type or *Sbno2*$^{-/-}$ mice. Chimeric wild-type mice lacking Sbno2 in their hematopoietic system showed significantly increased bone volume per tissue volume and decreased osteoclast parameters with an unchanged bone formation rate (Fig. 3, A and B). Next, we irradiated *Sbno2*$^{-/-}$ mice and reconstituted them with bone marrow from wild-type or *Sbno2*$^{-/-}$ mice. As expected, chimeric knockout mice having wild-type bone marrow showed decreased bone volume per tissue volume and

and *Sbno2*$^{-/-}$ mice. Oc.S/BS, osteoclast surface per bone surface; Oc.N/BS, osteoclast number per bone surface. (I) Bone erosion parameters in the metaphyseal portion of tibias from wild-type and *Sbno2*$^{-/-}$ mice. ES/BS, eroded surface per bone surface. (J) Numbers of nuclei per osteoclast in the trabecular area of tibias (top: TRAP staining of the metaphyseal portion of tibias) (K) Ruffled border formation of osteoclast in 10-wk old *Sbno2*$^{-/-}$ mice. Arrowheads, osteoclasts. Bar, 5 μm. (L) Serum concentrations of TRACP5b and CTX in 10-wk-old wild-type and *Sbno2*$^{-/-}$ mice. (M) Serum concentrations of RANKL and OPG in 10-wk-old wild-type and *Sbno2*$^{-/-}$ mice. (N) Osteoblast and bone formation parameters in the metaphyseal portion of tibias from 10-wk-old wild-type and *Sbno2*$^{-/-}$ mice. Ob.S/BS, osteoblast surface per bone surface; BFR, bone formation rate; MAR, mineral apposition rate. (O) Serum concentrations of ALP in 10-wk-old wild-type and *Sbno2*$^{-/-}$ mice. (P) Muscle tissues from 10-wk-old wild-type and *Sbno2*$^{-/-}$ mice were dissected from wild-type and *Sbno2*$^{-/-}$ mice, and stained by H&E (top: longitudinal view; bottom: axial view of the femoral muscle). Bar, 50 μm. BV/TV, bone volume per tissue volume; Tb.Th, trabecular bone thickness; Tb.N, trabecular bone number; Tb.Sp, trabecular bone spacing. Error bars, SE. *, $P < 0.05$, $n = 4$–5/group.

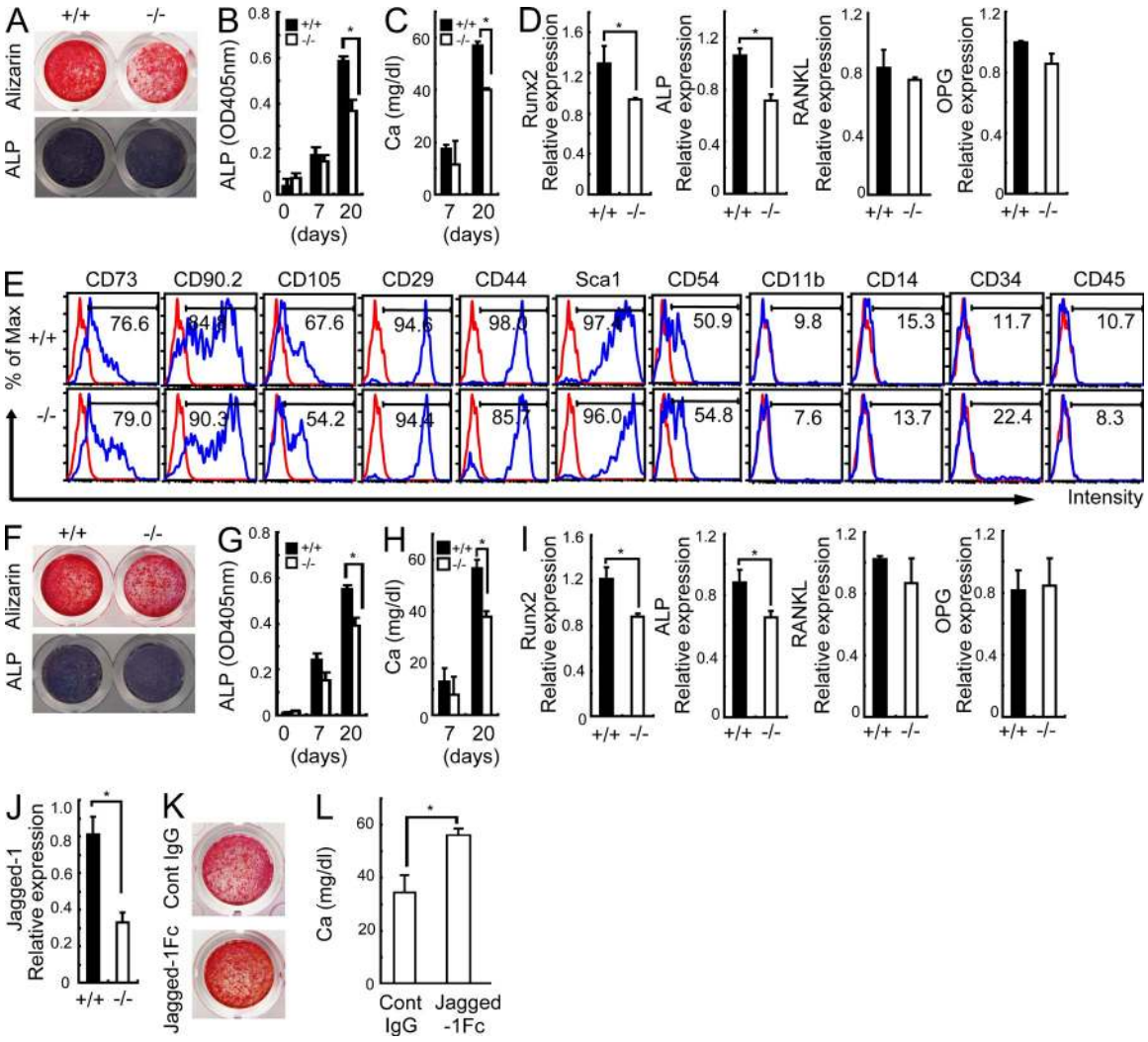

Figure 4. Impaired differentiation in *Sbno2*$^{-/-}$ osteoblasts. (A) Calvariae from wild-type and *Sbno2*$^{-/-}$ mice were treated with an osteoblast-inducer reagent for 20 d. Representative images of calcified nodules and ALP activities are indicated. (B and C) Calvariae from wild-type and *Sbno2*$^{-/-}$ mice were treated with an osteoblast-inducer reagent for the indicated number of days. ALP (B) and calcium (C) concentrations were measured. (D) qPCR analysis of Runx2, ALP, RANKL, and OPG in calvarial cells from A. (E) Immunophenotypic characterization of MSCs from wild-type or *Sbno2*$^{-/-}$ compact bone. (F) MSCs from wild-type and *Sbno2*$^{-/-}$ mice were treated with an osteoblast-inducer reagent for 20 d. Representative images of calcified nodules and ALP activities are indicated. (G and H) MSCs from wild-type and *Sbno2*$^{-/-}$ mice were treated with an osteoblast-inducer reagent for the indicated number of days. ALP (G) and calcium (H) concentrations were measured. (I) qPCR analysis of Runx2, ALP, RANKL, and OPG in MSC-derived cells from F. (J) qPCR analysis of Jagged-1 in calvarial osteoblasts from wild-type and *Sbno2*$^{-/-}$ mice. (K) Calvariae from *Sbno2*$^{-/-}$ mice stimulated with plate-bound Jagged1-Fc or control IgG. After incubation with an osteoblast-inducer reagent for 15 d, calcified nodules were stained. (L) Calcium concentrations in K were measured. Results in all panels are representative of two independent experiments. Error bars, SE. *, $P < 0.05$, $n = 3$.

increased osteoclast parameters with an unchanged bone formation rate (Fig. 3, A and B). Thus, these findings clearly indicate that the increased bone mass in mice with Sbno2 deficiency is solely a result of osteoclasts, and *Sbno2*$^{-/-}$ mice suffer from low-turnover osteopetrosis.

Impaired osteoblastogenesis in Sbno2$^{-/-}$ mice

Next, to check whether osteoblastogenesis of *Sbno2*$^{-/-}$ cells is abnormal, we cultured calvarial osteoblasts and found that *Sbno2*$^{-/-}$ osteoblasts exhibited a 20% decrease in the expression levels of Runx2 and ALP, as well as in bone nodule formation, compared with wild-type osteoblasts (Fig. 4, A–D). We also studied the population of mesenchymal stem cells (MSCs) from femurs and found that the Sbno2 deficiency had no effect on the expression levels of MSC markers (Fig. 4 E). In contrast, *Sbno2*$^{-/-}$ MSC-derived osteoblasts exhibited a slight impairment of differentiation (Fig. 4, F–I). Next, because Sbno2 is a Notch-related gene, we examined the expression levels of Notch family genes and found that the Jagged1 expression level was lower in Sbno2-deficient calvarial osteoblasts than in wild-type osteoblasts (Fig. 4 J). It was recently reported that Jagged1 enhances osteoblastogenesis (Nobta et al., 2005;

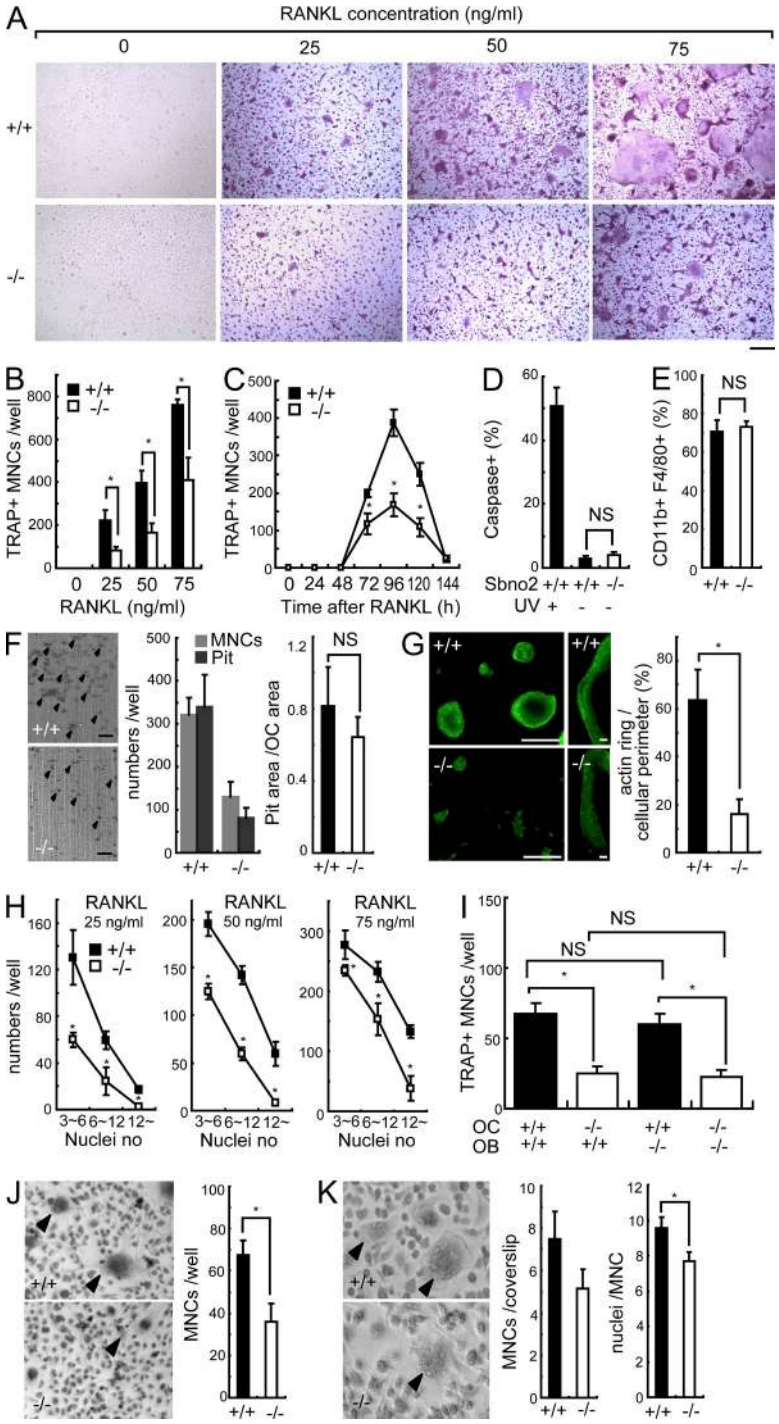

Figure 5. Impaired multinucleation of *Sbno2*$^{-/-}$ osteoclasts. (A) MDMs from wild-type and *Sbno2*$^{-/-}$ mice were cultured in the presence of the indicated RANKL concentrations. Representative TRAP staining is shown. Bar, 200 µm. (B) MDMs from wild-type and *Sbno2*$^{-/-}$ mice were cultured in the presence of the indicated RANKL concentrations. After 4 d, TRAP^{+} MNCs (more than three nuclei) were counted. (C) MDMs from wild-type and *Sbno2*$^{-/-}$ mice were cultured in the presence of 50 ng/ml RANKL, and sequential TRAP staining was performed to count the numbers of osteoclasts. (D) Apoptosis of wild-type and *Sbno2*$^{-/-}$ MDMs. Caspases were stained using a Poly Caspase Assay kit (ImmunoChemistry Technologies), and the numbers of caspase-positive cells were counted under a fluorescence microscope. (E) Analysis of wild-type and *Sbno2*$^{-/-}$ MDMs using the F4/80 and CD11b markers. (F) Resorption pits (analyzed by scanning electron microscope, arrowheads) from wild-type and *Sbno2*$^{-/-}$ osteoclasts. MDMs were plated on dentine slice and cultured with 50 ng/ml RANKL for 5 d. Pit numbers and multinucleated cell numbers were counted (middle). Resorption area (right) was determined using Image J. Bar, 100 µµm. (G) F-actin was stained with phalloidin. Bars: (left) 100 µm; (right) 5 µm. (H) MDMs from wild-type and *Sbno2*$^{-/-}$ mice were cultured in the presence of 25, 50, or 75 ng/ml RANKL. After 4 d, the number of nuclei in TRAP^{+} cells was analyzed. (I) Bone marrow cells (OC) and calvariae (OB) were cocultured in the presence of 1α,25(OH)2D3 for 8 d. TRAP^{+} MNCs were counted. (J) MDMs from wild-type and *Sbno2*$^{-/-}$ mice were cultured in the presence of 100 ng/ml IL-4. After 4 d, TRAP^{+} MNCs (more than three nuclei) were counted. Arrowheads indicate MNCs. (K) In vivo foreign body formation was induced by subcutaneous insertion of coverslips. After 4 d, coverslips were harvested and stained by hematoxylin and eosin. MNCs/ coverslips (n = 6) and numbers of nuclei/MNC (wild-type: n = 45, *Sbno2*$^{-/-}$: n = 31) were quantified. Arrowheads indicate MNCs. Results are representative of four (A–C) or three (D–J) independent experiments. Error bars, SE. *, $P < 0.05$, n = 4, unless indicated.

Osathanon et al., 2013). To determine if Jagged1 stimulation could rescue the impaired osteoblast differentiation resulting from Sbno2 deficiency, we cultured Sbno2-deficient calvarial osteoblasts on recombinant Jagged1-Fc protein-coated dishes. Notably, Jagged1 stimulated *Sbno2*$^{-/-}$ osteoblasts to exhibit increased differentiation and bone nodule formation (Fig. 4, K and L). These findings indicate that not only is osteoclast formation impaired, but osteoblastogenesis is partially decreased in *Sbno2*$^{-/-}$ cells.

Impaired fusion in Sbno2$^{-/-}$ osteoclasts

To evaluate the role of Sbno2 in osteoclastogenesis, we analyzed in vitro osteoclastogenesis using wild-type and *Sbno2*$^{-/-}$ MDMs (Fig. 5, A–C). We treated MDMs with increasing concentrations of RANKL, and TRAP-positive multinucleated cells were identified as mature osteoclasts after 4 d. RANKL-induced osteoclastogenesis (Fig. 5, A–C) and actin ring formation (Fig. 5 G) were impaired in *Sbno2*$^{-/-}$ cells, compared with those in wild-type cells. Although the number of bone

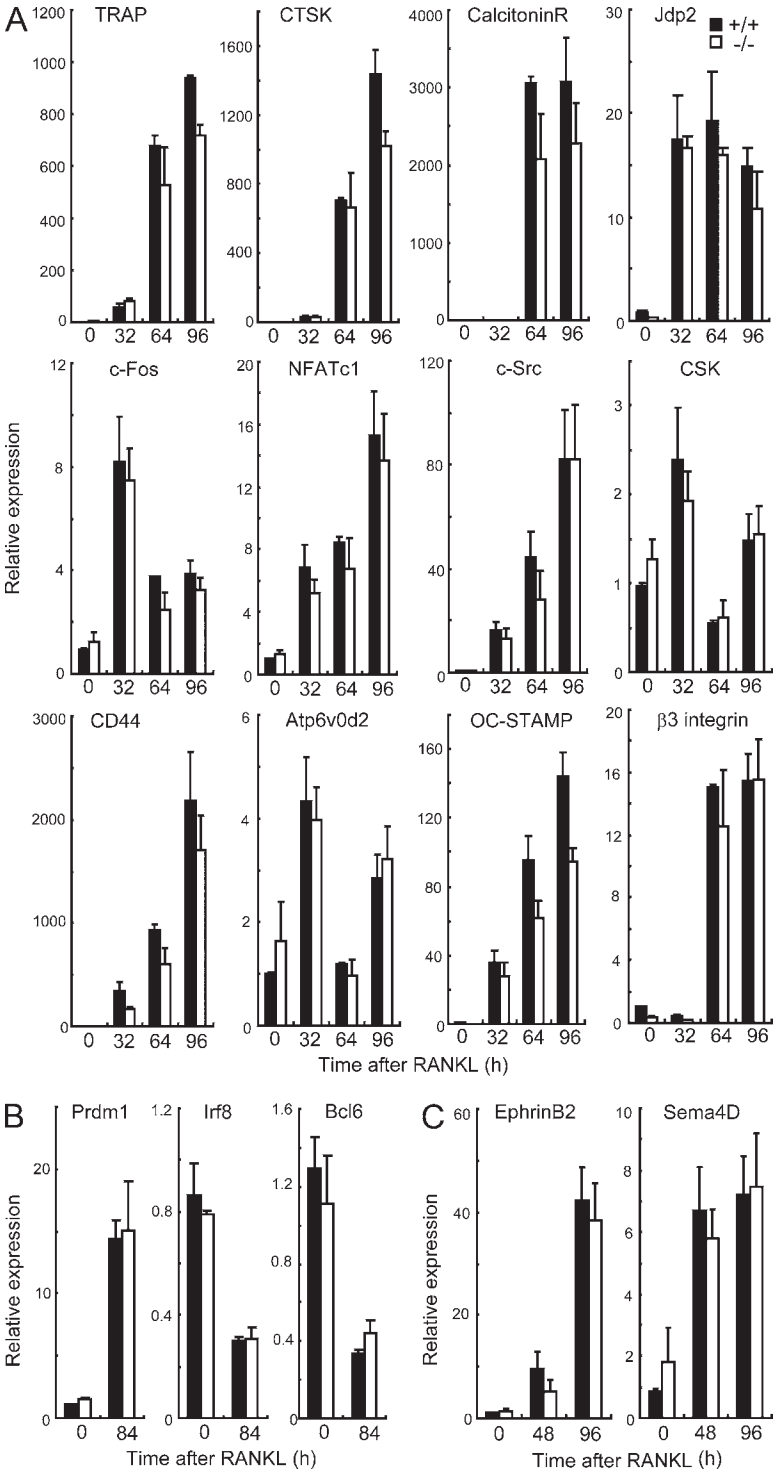

Figure 6. Osteoclast differentiation markers are normal in *Sbno2*$^{-/-}$ osteoclasts. (A) MDMs from wild-type and *Sbno2*$^{-/-}$ mice were cultured in the presence of 50 ng/ml RANKL. Cells were harvested in the indicated times, and TRAP, CTSK, calcitonin receptor, Jdp2, c-Fos, NFATc1, c-Src, CSK, CD44, Atp6v0d2, OC-STAMP, and β3-integrin levels were measured by qPCR. (B) qPCR analysis of Prdm1, Irf8, and Bcl6 levels in wild-type and *Sbno2*$^{-/-}$ MDMs stimulated with 50 ng/ml RANKL for 84 h. (C) MDMs from wild-type and *Sbno2*$^{-/-}$ mice were cultured in the presence of 50 ng/ml RANKL. Cells were harvested in the indicated times, and ephrin B2 and Sema4D levels were measured by qPCR. Results are representative of three (A and B) or two (C) independent experiments. Error bars, SE, $n = 3$.

resorption pits generated by *Sbno2*$^{-/-}$ osteoclasts was significantly reduced (Fig. 5 F), to an extent that was correlated with the reduction in TRAP^{+} multinuclear cell (MNC) numbers (Fig. 5 F), the area of resorption pits generated by the *Sbno2*$^{-/-}$ osteoclasts was similar to that generated by wild-type osteoclasts (Fig. 5 F). Thus, these data suggest that Sbno2$^{-/-}$ osteoclasts are functionally normal. Notably, *Sbno2*$^{-/-}$ osteoclasts had decreased numbers of nuclei and were smaller in size (Fig. 5 H). This defect was not due to a failure of osteoclast precursor characters (Fig. 5, D and E) or *Sbno2*$^{-/-}$ osteoblasts to support osteoclast differentiation but appeared to result from the loss of Sbno2 in MDMs (Fig. 5 I). Additionally, giant cell multinucleation induced in vitro by IL-4 and foreign body giant cell multinucleation induced in vivo by subcutaneous insertion of

coverslips were impaired in *Sbno2*$^{-/-}$ mice (Fig. 5, J and K). We also examined the expression levels of various osteoclastogenic genes using qPCR. At every time point, the expression levels of TRAP, CTSK, calcitonin receptor, Jdp2, c-Fos, NFATc1, c-Src, c-Src tyrosine kinase (CSK), CD44, Atp6v0d2, OC-STAMP, and β3-integrin were almost comparable between Sbno2-deficient osteoclasts and wild-type controls (Fig. 6 A). Furthermore, expression levels of Blimp1, which is the negative regulator of osteoclastogenesis, and its target genes (Ifr8 and Bcl6) were normal (Fig. 6 B). Additionally, we examined the expression levels of osteoclast–osteoblast coupling factors, such as ephrin B2 and Sema4D, and found them to be comparable between Sbno2-deficient osteoclasts and wild-type controls (Fig. 6 C). These findings strongly support the idea that osteoclast fusion, but not differentiation, is diminished in *Sbno2*$^{-/-}$ mice.

Sbno2 regulates DC-STAMP expression

The expression level of Sbno2 was significantly increased after RANKL stimulation in MDMs (Fig. 7 A). This transcriptional induction was dependent on c-Fos and its downstream target Jdp2 (based on c-Fos siRNA knockdown and analysis of Jdp2-deficient cells, Fig. 7, B and C) but not on NFATc1 (based on NFATc1 inhibition by FK506 treatment, Fig. 7 D). To reveal the mechanisms underlying the decreased fusion resulting from Sbno2 deficiency, we evaluated the activation of RANKL signaling. First, to rule out the possibility that differential RANK and c-fms expression was responsible for the abnormal phenotype in *Sbno2*$^{-/-}$ mice, we examined their expression levels in MDMs (Fig. 7 E). RANK and c-fms mRNA levels were comparable between wild-type and *Sbno2*$^{-/-}$ MDMs (Fig. 7 E). We also evaluated the activation of NFATc1 and NF-κB in response to RANKL, revealing that DNA binding of these transcription factors to their promoter was normal in *Sbno2*$^{-/-}$ MDMs (Fig. 7 F). Next, we quantified RANKL-induced calcium oscillations in wild-type and *Sbno2*$^{-/-}$ MDMs (Fig. 7 G). However, no difference was identified between genotypes (Fig. 7 G). In contrast, the level of DC-STAMP, a molecule critical for osteoclast fusion, was drastically decreased in *Sbno2*$^{-/-}$ osteoclasts (Fig. 7 H). As expected, DC-STAMP expression was also decreased in *Jdp2*$^{-/-}$ osteoclasts (Fig. 7 B). To gain an insight into the mechanism underlying the regulation of DC-STAMP by Sbno2, we first examined the MITF occupancy of the DC-STAMP promoter (Fig. 7 I). MITF is a critical transcription factor for DC-STAMP induction (Courtial et al., 2012) and, as predicted, MITF binding to the DC-STAMP promoter was impaired in *Sbno2*$^{-/-}$ osteoclasts (Fig. 7 I). It was recently reported that the transcription factor Tal1 is present on the DC-STAMP promoter, inhibiting its access by MITF (Courtial et al., 2012). Tal1 occupancy of the DC-STAMP promoter was decreased after RANKL stimulation in wild-type MDMs (Fig. 7 I). In contrast, such occupancy was sustained in response to RANKL stimulation in *Sbno2*$^{-/-}$ MDMs (Fig. 7 I). DC-STAMP expression is also known to be regulated by PU.1, NFATc1, c-Fos, and NF-κB, but the recruitment of these transcription factors to the DC-STAMP promoter was almost comparable between Sbno2-deficient osteoclasts and wild-type controls (Fig. 7 I). To examine whether increased DC-STAMP expression could rescue the fusion defect in *Sbno2*$^{-/-}$ cells, *Sbno2*$^{-/-}$ MDMs were transduced with a DC-STAMP retrovirus, and then stimulated by RANKL (Fig. 6, J–L). Notably, DC-STAMP–transduced *Sbno2*$^{-/-}$ MDMs generated significantly more and larger osteoclasts than *Sbno2*$^{-/-}$ MDMs, with the number and size of osteoclasts produced being comparable with the number and size of those produced by wild-type MDMs (Fig. 6, J–L). Collectively, these findings clearly indicate that the impaired DC-STAMP expression is the cause of the fusion defect in *Sbno2*$^{-/-}$ osteoclasts. Next, because Tal1 binding on the DC-STAMP promoter was sustained in response to RANKL stimulation in *Sbno2*$^{-/-}$ MDMs, we predicted that Sbno2 may inhibit Tal1 occupancy of the DC-STAMP promoter, and such a hypothesis prompted us to examine binding of Sbno2 to Tal1. Intriguingly, an association between Sbno2 and Tal1 was identified by immunoprecipitation of extracts from mouse primary MDMs (Fig. 7 M). Additionally, it seems that conserved domains in Sbno2 (aa 1-100, P loop containing NTP hydrolase pore 1; aa 501-1,000, DExD/H box groups helicase C domains) are not required for the interaction to Tal1 (Fig. 7 N). Furthermore, knockdown of Tal1 in *Sbno2*$^{-/-}$ MDMs significantly rescued the fusion deficiency in response to RANKL stimulation (Fig. 7, O–R). Based on these data, we further examined the effect of Sbno2 on the transcriptional activity of MITF. For this experiment, we used a luciferase reporter plasmid driven by the DC-STAMP promoter (Fig. 7 S). Only overexpression of MITF activated this promoter, whereas simultaneous expression with Tal1 reduced the promoter activity to control levels (Fig. 7 S). In contrast, simultaneous expression of Tal1 and Sbno2 significantly cancelled the inhibitory effect of Tal1 on the DC-STAMP promoter (Fig. 7 S). Together, these findings imply that Sbno2 inhibits the DC-STAMP repressive activity of Tal1 by directly binding to Tal1 and enhancing MITF access to the DC-STAMP promoter.

DISCUSSION

In contrast to the normal host defense and NF-κB activation, *Sbno2*$^{-/-}$ mice exhibited a severe osteopetrotic phenotype. Histomorphometric analysis indicated a reduction in the osteoclast surface/bone surface ratio in *Sbno2*$^{-/-}$ mice. In vitro RANKL-induced osteoclast multinucleation was also impaired, but activation of osteoclastogenic transcription factors such as NFATc1, NF-κB, and c-Fos was normal in *Sbno2*$^{-/-}$ cells. Furthermore, our data demonstrated that expression of DC-STAMP, a molecule critical for osteoclast fusion, was reduced in *Sbno2*$^{-/-}$ cells, and that impaired cell fusion of *Sbno2*$^{-/-}$ osteoclasts was rescued by DC-STAMP. Unfortunately, the meaning of the discrepancy between the TLR-induced NF-κB activation levels in Sbno2-deficient cells and the implications of previous in vitro Sbno2 overexpression reporter assays is enigmatic. However, the possibility that Sbno2 plays some role in IL-10 responses in some cell types cannot be ruled out. Further cell type–specific studies are needed to identify the

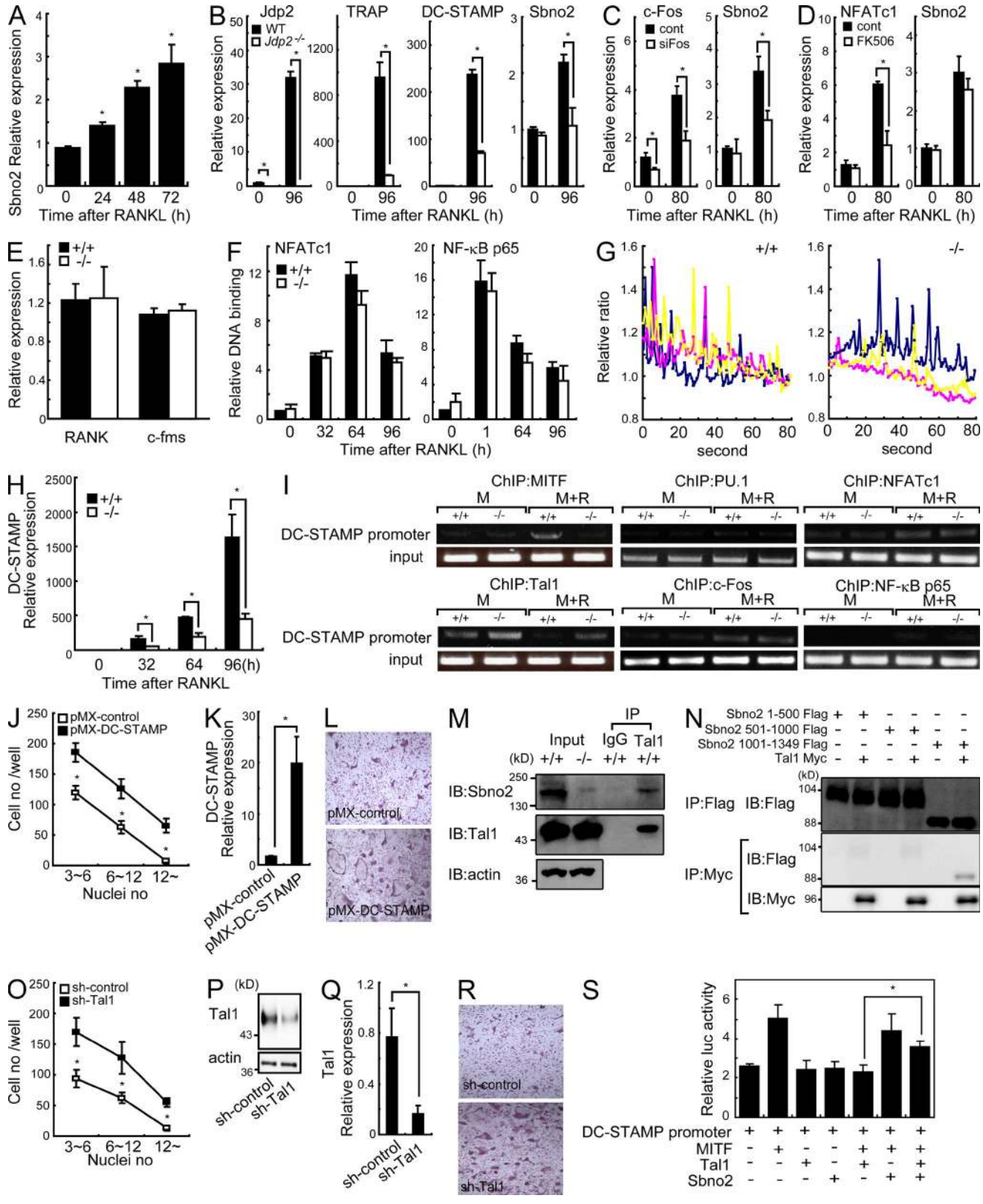

Figure 7. Sbno2 plays a key role in fine tuning DC-STAMP expression. (A) MDMs from wild-type mice were treated with 100 ng/ml RANKL for the indicated times. Sbno2 mRNA levels were measured by qPCR. (B) qPCR analysis of Jdp2, TRAP, DC-STAMP, and Sbno2 in wild-type and *Jdp2*$^{-/-}$ MDMs stimulated with 50 ng/ml RANKL. (C) MDMs were transfected with control siRNA (cont) or c-Fos–specific siRNA (siFos) and stimulated with 50 ng/ml RANKL. c-Fos and Sbno2 levels were measured by qPCR. (D) MDMs were treated with 3 µg/ml FK506 (FK506) or DMSO (cont) and stimulated with 50 ng/ml

importance of Sbno2 within the signaling pathways of the innate immune system.

It has been reported that bone remodeling in DC-STAMP–deficient mice is regulated in an uncoupled manner, and decreased bone resorption and increased bone formation are observed (Iwasaki et al., 2008). However, despite decreased DC-STAMP expression, the bone metabolism in *Sbno2*$^{-/-}$ mice appeared to be regulated in a coupled manner because of the decreased osteoblastogenesis. Thus, the osteopetrosis in *Sbno2*$^{-/-}$ mice was caused by decreased bone turnover. Furthermore, our findings indicate that the expression level of Jagged1 is decreased in Sbno2-deficient osteoblasts, and Jagged1 stimulation could prevent the differentiation impairment of Sbno2-deficient osteoblasts. Unfortunately, we cannot explain the precise mechanisms underlying the impaired expression of Jagged1 in Sbno2-deficient osteoblasts. Further studies are needed to explore the role of Sbno2 in osteoblasts, but our discoveries provide a motivation for studies aimed at elucidating the importance of Sbno2 in mesenchymal lineages. Additionally, despite DC-STAMP–deficient mice exhibiting no reproductive defects (Yagi et al., 2005), a partial distortion of male transmission frequency was suspected among offspring derived from Sbno2 heterozygous intercrosses. Furthermore, it has been reported that cellular fusion process is important in some tissues such as uterus and fertilization of egg. Thus, our observations clearly indicate the importance of Sbno2 in osteoclast fusion and also suggest the need to identify the importance of Sbno2 in other fusion tissues.

In this study, we found that Sbno2 inhibited the DC-STAMP–repressive activity of Tal1 by directly binding to Tal1 and enhancing MITF access to the DC-STAMP promoter. During osteoclastogenesis, the protein level of Tal1 was significantly elevated. In contrast, Tal1 occupancy of the DC-STAMP promoter was decreased after RANKL stimulation (Courtial et al., 2012). Because the expression level of Sbno2 was increased during osteoclastogenesis, it is plausible that the Sbno2 level regulates Tal1 binding to the DC-STAMP promoter. Further investigation is needed aimed at providing a precise mechanistic understanding of Sbno2's function in osteoclastogenesis, but our data clearly indicate that Sbno2 plays a key role in fine-tuning osteoclast fusion, and they provide a basis for Sbno2-targeted therapeutic approaches to treat osteoporosis without affecting the innate immune system.

MATERIALS AND METHODS

Generation of *Sbno2*$^{-/-}$ mice. A gene-targeting vector containing three LoxP sites flanking exons 19–25, a neomycin resistance cassette, and the gene encoding herpes simplex virus thymidine kinase, driven by the promoter of the gene encoding phosphoglycerate kinase, was constructed (Fig. 1 C). The targeting vector was electroporated into embryonic stem cells and clones resistant to G418 and ganciclovir were screened for homologous recombination by PCR. Chimeric progeny were crossed with the CAG-Cre deleter strain to generate null animals. *Sbno2*$^{-/-}$ mice on the 129Sv x C57BL/6 background and their littermate were used. Southern blot analysis was also performed and mRNA levels of Sbno2 in macrophages were confirmed by PCR (Fig. 1, D and E). All animal experiments were performed with the approval of the Animal Research Committee of the Research Institute for Microbial Diseases (Osaka University).

Generation of bone marrow chimeric mice. 1×10^7 10-wk-old bone marrow cells from *Sbno2*$^{-/-}$ and control wild-type mice were intravenously injected into lethally irradiated 4-wk-old recipient mice. Mice were analyzed at 7 wk after bone marrow transplantation.

Cells, pathogens, and reagents. B cells and T cells were isolated from splenocytes by positive selection with anti-B220 and anti–Thy-1.2 magnetic beads (Miltenyi Biotec), respectively. Splenic DCs were isolated by positive selection with anti-CD11c magnetic beads (Miltenyi Biotec). Splenic CD11b$^+$ macrophages were sorted by a FACSAria (BD). Antibodies for FACS analysis were purchased from BD, and cells were stained with the indicated antibodies. Data were acquired with a FACSCalibur (BD) and analyzed by Tree Star. *S. aureus* 834, designated here as *S. aureus*, was provided by A. Nakane (Hirosaki University School of Medicine, Aomori, Japan). *S. aureus* was cultured on tryptic soy broth agar plates at 37°C for 24 h before use. Recombinant mouse Jagged-1:Fc chimeric protein was purchased from Enzo Life Sciences. Lipopolysaccharide from *Salmonella minnesota* strain Re-595 was purchased from Sigma-Aldrich. Poly(I:C) was purchased from GE Healthcare. MALP-2 was prepared as previously described (Takeuchi et al., 2000). R-848 was provided by the Pharmaceuticals and Biotechnology Laboratory of the Japan Energy Corporation (Toda, Saitama, Japan). The CpG oligonucleotide (Kawagoe et al., 2008) and a synthetic *N*-palmitoyl-*S*-dipalmitoylglyceryl (Pam_3) Cys-Ser-$(Lys)_4$ (CSK_4; Takeuchi et al., 2002) were generated as described previously. The TRACP5b ELISA kit (Immunodiagnostic Systems), cross-linked C-telopeptide of Type I collagen (CTX) ELISA kit (USCN Life Science), RANKL ELISA

RANKL. NFATc1 and Sbno2 levels were measured by qPCR. (E) RANK and c-fms mRNA levels in unstimulated MDMs from wild-type and *Sbno2*$^{-/-}$ mice were measured by qPCR. (F) MDMs from wild-type mice were treated with 150 ng/ml RANKL for the indicated times. Nuclear extracts were harvested and DNA-binding activity of NFATc1 and NF-κB p65 were measured using a TransAM Transcription Factor Assay kit. (G) MDMs from wild-type and *Sbno2*$^{-/-}$ mice were treated with 100 ng/ml RANKL for 24 h and Ca^{2+} imaging was performed. Three representative traces of change in the fura-2 fluorescence ratio in cells are shown. (H) qPCR analysis of DC-STAMP level in wild-type and *Sbno2*$^{-/-}$ MDMs stimulated with 50 ng/ml RANKL for the indicated number of hours. (I) Chromatin immunoprecipitation analyses with indicated antibodies of lysates from wild-type and *Sbno2*$^{-/-}$ MDMs stimulated with or without 100 ng/ml RANKL for 84 h. DNA fragments of the DC-STAMP promoter region were detected by PCR. (J–L) Effect of exogenous DC-STAMP expression on the osteoclastogenesis of *Sbno2*$^{-/-}$ MDMs stimulated with 50 ng/ml RANKL for 4 d. Nuclei numbers (J) in TRAP$^+$ cells were analyzed ($n = 4$). DC-STAMP expression levels were measured by qPCR (K) and representative TRAP staining is shown (L). (M) Immunoprecipitation of wild-type MDM lysates. After anti-Tal1 and control IgG immunoprecipitation, immunoprecipitates were analyzed by Western blotting with anti-Sbno2 and anti-Tal1 antibodies. *Sbno2*$^{-/-}$ MDMs were also used as Input. (N) Association between Sbno2 and Tal1 was analyzed by coimmunoprecipitation. HEK293T cells were transfected with the following constructs: Sbno2 1–500 Flag (aa residues 1–500), Sbno2 501–1000 Flag (aa residues 501–1,000), Sbno2 1001–1349 (aa residues 1,001–1,349), and Tal1 Myc. (O–R) Effect of Tal1 knockdown on the osteoclastogenesis of *Sbno2*$^{-/-}$ MDMs stimulated with 50 ng/ml RANKL for 4 d. Nuclei numbers (O) in TRAP$^+$ cells were analyzed ($n = 4$). DC-STAMP expression levels were measured by qPCR (P) and Western blotting (Q). Representative TRAP staining is shown (R). (S) Luciferase assays examining the effects of Sbno2 on the transcriptional activity of DC-STAMP. Results are representative of three (A–E and H–S) or two (F and G) independent experiments. Error bars, SE. *, $P < 0.05$, $n = 3$ unless indicated.

kit (MTR00; R&D Systems), and OPG ELISA kit (MOP00; R&D Systems) were purchased. ELISA kits for IL-6, TNF, and IL-12 were purchased from R&D Systems. The ALP quantification kit was purchased from LabAssay (Wako). Nuclear extracts were prepared as described previously (Kawagoe et al., 2009), and the DNA-binding activities of NF-κB p65 and NFATc1 were analyzed by a TransAM Transcription Factor Assay kit (Active Motive).

Analysis of bone phenotype. To measure bone formation, double calcein labeling was performed. We intraperitoneally injected calcein (16 mg/kg body weight; Wako) into mice and repeated the dose 72 h later. We killed the mice 24 h after the second injection, and femurs were fixed with 70% ethanol before being subjected to morphometric analysis. Three-dimensional μ-CT analysis of femurs was conducted using a Scan-Xmate RB080SS110 system (Comscan Techno Co., Ltd) and bone structural indices were measured using TRI/3D-Bon software (Ratoc System Engineering Co., Ltd). Bone micro-architectural parameters were analyzed in the trabecular regions from 0.1 to 1.5 mm away from the chondro-osseous junction. For histomorphometric analysis, tibias were fixed with 70% ethanol, stained with Villanueva Bone Stain (Wako), and then embedded in MMA. Serial longitudinal sections (6-mm thickness) were prepared using a microtome RM2255 (Leica) and then analyzed by a Histometry RT Camera (System Supply Co., Ltd). Bone morphometric parameters were defined as previously described (Parfitt et al., 1987).

In vivo infection. *S. aureus* was cultured in tryptic soy broth for 15 h at 37°C. Mice were infected intravenously with 0.2 ml of a PBS solution containing 3×10^7 *S. aureus* cells. Mice were monitored for 5 d, and serum cytokine levels were measured as previously described (Maruyama et al., 2007).

Osteoclast/osteoblast culture and functional evaluation. MDMs were generated as described previously (Maruyama et al., 2006) and induced to differentiate into osteoclasts in the presence of 25 ng/ml M-CSF and various incubation times and concentrations of RANKL (R&D Systems). TRAP staining was performed as described previously (Maruyama et al., 2012b). For the pit assay, MDMs were cultured on dentine slices (Wako). After 5 d, plates were immersed for 3 h in 1 M NH_4OH, and resorption pits were observed by scanning electron microscopy (MiniScope TM-1000; Hitachi). Calvariae from 2-d-old mice were digested in α-MEM containing 0.1% collagenase and 0.2% dispase at 37°C for 20 min. MSCs from femur compact bone were harvested, as previously described (Zhu et al., 2010). Calvarial cells or MSCs were then expanded in α-MEM containing 10% FCS. For induction of osteoblastogenesis, primary calvarial cells were plated and medium supplemented with an osteoblast-inducer reagent was added (Takara Bio Inc.). In some experiments, culture plate–bound Jagged-1:Fc chimeric protein (Enzo Life Sciences) or control IgG was fabricated using a previously described indirect affinity immobilization method (Beckstead et al., 2006, 2009) and calvarial cells were plated on it. The osteoblast-inducer reagent–containing medium was changed every 3 d. After 7 or 20 d, calcified nodules and ALP were stained using a Calcified Nodule Staining kit (AK-21; Primary Cell) and a TRAP/ALP staining kit (Wako), respectively. Calcified nodules were dissolved in 0.5 M HCl solution and calcium concentration was measured using a kit (Metalloassay LS-MPR; AKJ Global Technology). For osteoclast/osteoblast co-culture, bone marrow cells (3×10^5) and primary calvarial osteoblasts (5×10^5) were isolated and cultured in 24-well plates containing α-MEM supplemented with 10% FCS for 8 d in the presence of 10 nM $1\alpha,25(OH)_2D_3$. After the culture, the cells were fixed and stained for TRAP to evaluate the numbers of osteoclasts.

Giant cell formation. For in vitro giant cell formation, MDMs were cultured in the presence of 50 ng/ml M-CSF. After 3 d, 100 ng/ml IL-4 (PeproTech) was added and cultured for additional 4 d. Giant cell formation in vivo was induced as previously described (Gonzalo et al., 2010). In brief, 12-mm-diameter coverslips were implanted subcutaneously in the backs of mice. After 4 d, coverslips were harvested and stained by hematoxylin and eosin.

Quantitative real-time PCR analysis. RNA was extracted from cells using TRIzol (Invitrogen), and reverse transcription was performed using ReverTra Ace (Toyobo Co., Ltd.). Quantitative real-time PCR (qPCR) was performed with an ABI PRISM 7500 using TaqMan Assay-on-demand primers (Applied Biosystems).

Intracellular calcium imaging. MDMs were plated on poly-L-lysine–coated glass-bottom dishes and loaded with 5 μM Fura-2/AM for 30 min in loading solution (115 mM NaCl, 5.4 mM KCl, 1 mM $MgCl_2$, 2 mM $CaCl_2$, 20 mM Hepes, and 10 mM glucose, pH 7.42). Fura-2 fluorescence images were analyzed as described previously (Kuroda et al., 2008).

Viral gene transfer/knockdown. DC-STAMP was cloned into the retroviral vector pMX-IRES. The construct was transfected into the packaging cell line PlatE, and viral supernatants were collected. Retroviral gene transduction of bone marrow cells was performed as previously described (Satoh et al., 2010). After transduction, cells were cultured for 3 d with M-CSF and then stimulated with RANKL for an additional 4 d to induce osteoclasts. Tal1 shRNA lentiviral particles (Santa Cruz Biotechnology, Inc.) and control shRNA lentiviral particles (Santa Cruz Biotechnology, Inc.) were purchased. For lentiviral gene transfer, MDMs were plated and virus was added to the well with polybrene. After 20 h, cells were stimulated with RANKL for an additional 4 d to induce osteoclasts.

Immunoblotting, immunoprecipitation, and chromatin immunoprecipitation assay. For immunoprecipitation, precleared cell lysates were incubated with protein A–Sepharose (GE Healthcare) containing 3 μg anti-Tal1 antibodies (H-60; Santa Cruz Biotechnology, Inc.) or rabbit polyclonal IgG (Y-11; Santa Cruz Biotechnology, Inc.) for 1 h at 4°C. The immunoprecipitants were washed, eluted, and then analyzed by Western blotting as described previously (Kawagoe et al., 2009). Proteins were detected using anti-Tal1 and anti-Sbno2 (K-15; Santa Cruz Biotechnology, Inc.) antibodies. Chromatin immunoprecipitation was performed as previously described (Satoh et al., 2010). After cells were fixed, chromatin was precipitated using anti-MITF (Abcam), anti-Tal1 (Abcam), anti-PU.1 (Santa Cruz Biotechnology, Inc.), anti–c-Fos (K25; Santa Cruz Biotechnology, Inc.), anti-NFATc1 (7A6; Santa Cruz Biotechnology, Inc.), and anti–NF-κB (C-20; Santa Cruz Biotechnology, Inc.) antibodies. Precipitated DNA was analyzed by PCR using primers that detect sequences containing the *dc-stamp* promoter, specifically: for MITF and Tal-1, 5′-GAGCTATGGGCTCATCCAGAAATC-3′ and 5′-AACTGGAAAAAGGAGCCACAGGTT-3′; for c-Fos and NFATc1, 5′-GGGGGTCCTCATTTCTACAACTCAT-3′ and 5′-GCCACATCAC-CCTGAATCAATCTT-3′; for PU.1, 5′-GAGCTATGGGCTCATCCA-GAAATC-3′ and 5′-AACTGGAAAAAGGAGCCACAGGTT-3′; and for NF-κB, 5′-AATGCTATCCCCAAAGTCCCCTAT-3′ and 5′-CTCGCG-AAGATCATACGCTCTAGT-3′ (Yagi et al., 2007; Courtial et al., 2012).

Luciferase reporter assay. The mouse DC-STAMP reporter plasmid has been described previously (Yagi et al., 2007). RAW264.7 cells were transfected with the DC-STAMP reporter plasmid and pCMV-RHL, as well as Tal-1, Sbno2, and MITF expression vectors using Lipofectamine 2000 (Invitrogen). After 36 h, luciferase activities of total cell lysates were measured using a Dual-Luciferase Reporter Assay System (Promega) as described previously (Iwasaki et al., 2011).

Statistical analysis. Student's *t* test was used to evaluate statistical significance, with significance set at $P < 0.05$. For survival curves, two groups were compared using a log-rank test.

We thank T. Miyamoto (Keio University School of Medicine, Tokyo, Japan) for providing the DC-STAMP reporter plasmid, E. Kamada and M. Kageyama for secretarial assistance, Y. Fujiwara and M. Kumagai for technical assistance, and T. Saitoh for participating in fruitful discussions.

This work was supported by the Special Coordination Funds of the Japanese Ministry of Education, Culture, Sports, Science, and Technology, grants from the Ministry of Health, Labor, and Welfare of Japan, and the Japan Society for the Promotion of Science (JSPS) through the Funding Program for World-Leading Innovative R&D on Science and Technology (FIRST Program), a grant from the

Osaka University MEET project, and a research fellowship from the JSPS for the Promotion of Science for Young Scientists.

The authors declare no competing financial interests.

K. Maruyama initiated, designed and performed most of the experiments. S. Uematsu generated Sbno2-deficient mice. T. Kondo, O. Takeuchi, M.M. Martino, and T. Kawasaki contributed to the experiments. The manuscript was written by K. Maruyama. S. Akira supervised overall research.

Submitted: 12 March 2013
Accepted: 25 July 2013

REFERENCES

Akira, S., S. Uematsu, and O. Takeuchi. 2006. Pathogen recognition and innate immunity. *Cell.* 124:783–801. http://dx.doi.org/10.1016/j.cell.2006.02.015

Beckstead, B.L., D.M. Santosa, and C.M. Giachelli. 2006. Mimicking cell-cell interactions at the biomaterial-cell interface for control of stem cell differentiation. *J. Biomed. Mater. Res. A.* 79:94–103.

Beckstead, B.L., J.C. Tung, K.J. Liang, Z. Tavakkol, M.L. Usui, J.E. Olerud, and C.M. Giachelli. 2009. Methods to promote Notch signaling at the biomaterial interface and evaluation in a rafted organ culture model. *J. Biomed. Mater. Res. A.* 91:436–446.

Chiu, Y.H., K.A. Mensah, E.M. Schwarz, Y. Ju, M. Takahata, C. Feng, L.A. McMahon, D.G. Hicks, B. Panepento, P.C. Keng, and C.T. Ritchlin. 2012. Regulation of human osteoclast development by dendritic cell-specific transmembrane protein (DC-STAMP). *J. Bone Miner. Res.* 27:79–92. http://dx.doi.org/10.1002/jbmr.531

Courtial, N., J.J. Smink, O.N. Kuvardina, A. Leutz, J.R. Göthert, and J. Lausen. 2012. Tal1 regulates osteoclast differentiation through suppression of the master regulator of cell fusion DC-STAMP. *FASEB J.* 26:523–532. http://dx.doi.org/10.1096/fj.11-190850

El Kasmi, K.C., A.M. Smith, L. Williams, G. Neale, A.D. Panopoulos, S.S. Watowich, H. Häcker, B.M. Foxwell, and P.J. Murray. 2007. Cutting edge: A transcriptional repressor and corepressor induced by the STAT3-regulated anti-inflammatory signaling pathway. *J. Immunol.* 179:7215–7219.

Franzoso, G., L. Carlson, L. Xing, L. Poljak, E.W. Shores, K.D. Brown, A. Leonardi, T. Tran, B.F. Boyce, and U. Siebenlist. 1997. Requirement for NF-kappaB in osteoclast and B-cell development. *Genes Dev.* 11:3482–3496. http://dx.doi.org/10.1101/gad.11.24.3482

Gonzalo, P., M.C. Guadamillas, M.V. Hernández-Riquer, A. Pollán, A. Grande-García, R.A. Bartolomé, A. Vasanji, C. Ambrogio, R. Chiarle, J. Teixidó, et al. 2010. MT1-MMP is required for myeloid cell fusion via regulation of Rac1 signaling. *Dev. Cell.* 18:77–89. http://dx.doi.org/10.1016/j.devcel.2009.11.012

Grigoriadis, A.E., Z.Q. Wang, M.G. Cecchini, W. Hofstetter, R. Felix, H.A. Fleisch, and E.F. Wagner. 1994. c-Fos: a key regulator of osteoclast-macrophage lineage determination and bone remodeling. *Science.* 266:443–448. http://dx.doi.org/10.1126/science.7939685

Iwasaki, H., O. Takeuchi, S. Teraguchi, K. Matsushita, T. Uehata, K. Kuniyoshi, T. Satoh, T. Saitoh, M. Matsushita, D.M. Standley, and S. Akira. 2011. The IκB kinase complex regulates the stability of cytokine-encoding mRNA induced by TLR-IL-1R by controlling degradation of regnase-1. *Nat. Immunol.* 12:1167–1175. http://dx.doi.org/10.1038/ni.2137

Iwasaki, R., K. Ninomiya, K. Miyamoto, T. Suzuki, Y. Sato, H. Kawana, T. Nakagawa, T. Suda, and T. Miyamoto. 2008. Cell fusion in osteoclasts plays a critical role in controlling bone mass and osteoblastic activity. *Biochem. Biophys. Res. Commun.* 377:899–904. http://dx.doi.org/10.1016/j.bbrc.2008.10.076

Karsenty, G., and E.F. Wagner. 2002. Reaching a genetic and molecular understanding of skeletal development. *Dev. Cell.* 2:389–406. http://dx.doi.org/10.1016/S1534-5807(02)00157-0

Kawagoe, T., S. Sato, K. Matsushita, H. Kato, K. Matsui, Y. Kumagai, T. Saitoh, T. Kawai, O. Takeuchi, and S. Akira. 2008. Sequential control of Toll-like receptor-dependent responses by IRAK1 and IRAK2. *Nat. Immunol.* 9:684–691. http://dx.doi.org/10.1038/ni.1606

Kawagoe, T., O. Takeuchi, Y. Takabatake, H. Kato, Y. Isaka, T. Tsujimura, and S. Akira. 2009. TANK is a negative regulator of Toll-like receptor signaling and is critical for the prevention of autoimmune nephritis. *Nat. Immunol.* 10:965–972. http://dx.doi.org/10.1038/ni.1771

Kawaida, R., T. Ohtsuka, J. Okutsu, T. Takahashi, Y. Kadono, H. Oda, A. Hikita, K. Nakamura, S. Tanaka, and H. Furukawa. 2003. Jun dimerization protein 2 (JDP2), a member of the AP-1 family of transcription factor, mediates osteoclast differentiation induced by RANKL. *J. Exp. Med.* 197:1029–1035. http://dx.doi.org/10.1084/jem.20021321

Khosla, S. 2009. Increasing options for the treatment of osteoporosis. *N. Engl. J. Med.* 361:818–820. http://dx.doi.org/10.1056/NEJMe0905480

Kuroda, Y., C. Hisatsune, T. Nakamura, K. Matsuo, and K. Mikoshiba. 2008. Osteoblasts induce Ca2+ oscillation-independent NFATc1 activation during osteoclastogenesis. *Proc. Natl. Acad. Sci. USA.* 105:8643–8648. http://dx.doi.org/10.1073/pnas.0800642105

Maruyama, K., Y. Takada, N. Ray, Y. Kishimoto, J.M. Penninger, H. Yasuda, and K. Matsuo. 2006. Receptor activator of NF-kappa B ligand and osteoprotegerin regulate proinflammatory cytokine production in mice. *J. Immunol.* 177:3799–3805.

Maruyama, K., G. Sano, N. Ray, Y. Takada, and K. Matsuo. 2007. c-Fos-deficient mice are susceptible to *Salmonella enterica* serovar Typhimurium infection. *Infect. Immun.* 75:1520–1523. http://dx.doi.org/10.1128/IAI.01316-06

Maruyama, K., M. Fukasaka, A. Vandenbon, T. Saitoh, T. Kawasaki, T. Kondo, K.K. Yokoyama, H. Kidoya, N. Takakura, D. Standley, et al. 2012a. The transcription factor Jdp2 controls bone homeostasis and antibacterial immunity by regulating osteoclast and neutrophil differentiation. *Immunity.* 37:1024–1036. http://dx.doi.org/10.1016/j.immuni.2012.08.022

Maruyama, K., T. Kawagoe, T. Kondo, S. Akira, and O. Takeuchi. 2012b. TRAF family member-associated NF-κB activator (TANK) is a negative regulator of osteoclastogenesis and bone formation. *J. Biol. Chem.* 287:29114–29124. http://dx.doi.org/10.1074/jbc.M112.347799

Motyckova, G., K.N. Weilbaecher, M. Horstmann, D.J. Rieman, D.Z. Fisher, and D.E. Fisher. 2001. Linking osteopetrosis and pycnodysostosis: regulation of cathepsin K expression by the microphthalmia transcription factor family. *Proc. Natl. Acad. Sci. USA.* 98:5798–5803. http://dx.doi.org/10.1073/pnas.091479298

Nobta, M., T. Tsukazaki, Y. Shibata, C. Xin, T. Moriishi, S. Sakano, H. Shindo, and A. Yamaguchi. 2005. Critical regulation of bone morphogenetic protein-induced osteoblastic differentiation by Delta1/Jagged1-activated Notch1 signaling. *J. Biol. Chem.* 280:15842–15848. http://dx.doi.org/10.1074/jbc.M412891200

Osathanon, T., P. Ritprajak, N. Nowwarote, J. Manokawinchoke, C. Giachelli, and P. Pavasant. 2013. Surface-bound orientated Jagged-1 enhances osteogenic differentiation of human periodontal ligament-derived mesenchymal stem cells. *J. Biomed. Mater. Res. A.* 101:358–367.

Parfitt, A.M., M.K. Drezner, F.H. Glorieux, J.A. Kanis, H. Malluche, P.J. Meunier, S.M. Ott, and R.R. Recker; Report of the ASBMR Histomorphometry Nomenclature Committee. 1987. Bone histomorphometry: standardization of nomenclature, symbols, and units. *J. Bone Miner. Res.* 2:595–610. http://dx.doi.org/10.1002/jbmr.5650020617

Satoh, T., O. Takeuchi, A. Vandenbon, K. Yasuda, Y. Tanaka, Y. Kumagai, T. Miyake, K. Matsushita, T. Okazaki, T. Saitoh, et al. 2010. The Jmjd3-Irf4 axis regulates M2 macrophage polarization and host responses against helminth infection. *Nat. Immunol.* 11:936–944. http://dx.doi.org/10.1038/ni.1920

Takayanagi, H., S. Kim, T. Koga, H. Nishina, M. Isshiki, H. Yoshida, A. Saiura, M. Isobe, T. Yokochi, J. Inoue, et al. 2002. Induction and activation of the transcription factor NFATc1 (NFAT2) integrate RANKL signaling in terminal differentiation of osteoclasts. *Dev. Cell.* 3:889–901. http://dx.doi.org/10.1016/S1534-5807(02)00369-6

Takeda, K., B.E. Clausen, T. Kaisho, T. Tsujimura, N. Terada, I. Förster, and S. Akira. 1999. Enhanced Th1 activity and development of chronic enterocolitis in mice devoid of Stat3 in macrophages and neutrophils. *Immunity.* 10:39–49. http://dx.doi.org/10.1016/S1074-7613(00)80005-9

Takeuchi, O., A. Kaufmann, K. Grote, T. Kawai, K. Hoshino, M. Morr, P.F. Mühlradt, and S. Akira. 2000. Cutting edge: preferentially the R-stereoisomer of the mycoplasmal lipopeptide macrophage-activating lipopeptide-2 activates immune cells through a toll-like receptor 2- and MyD88-dependent signaling pathway. *J. Immunol.* 164:554–557.

Takeuchi, O., S. Sato, T. Horiuchi, K. Hoshino, K. Takeda, Z. Dong, R.L. Modlin, and S. Akira. 2002. Cutting edge: role of Toll-like receptor 1 in mediating immune response to microbial lipoproteins. *J. Immunol.* 169:10–14.

Yagi, M., T. Miyamoto, Y. Sawatani, K. Iwamoto, N. Hosogane, N. Fujita, K. Morita, K. Ninomiya, T. Suzuki, K. Miyamoto, et al. 2005. DC-STAMP is essential for cell-cell fusion in osteoclasts and foreign body giant cells. *J. Exp. Med.* 202:345–351. http://dx.doi.org/10.1084/jem.20050645

Yagi, M., K. Ninomiya, N. Fujita, T. Suzuki, R. Iwasaki, K. Morita, N. Hosogane, K. Matsuo, Y. Toyama, T. Suda, and T. Miyamoto. 2007. Induction of DC-STAMP by alternative activation and downstream signaling mechanisms. *J. Bone Miner. Res.* 22:992–1001. http://dx.doi.org/10.1359/jbmr.070401

Zhu, H., Z.K. Guo, X.X. Jiang, H. Li, X.Y. Wang, H.Y. Yao, Y. Zhang, and N. Mao. 2010. A protocol for isolation and culture of mesenchymal stem cells from mouse compact bone. *Nat. Protoc.* 5:550–560. http://dx.doi.org/10.1038/nprot.2009.238